Seismic Evidence for Hotspot-Induced Buoyant Flow Beneath the Reykjanes Ridge

James B. Gaherty

Volcanic hotspots and mid-ocean ridge spreading centers are the surface expressions of upwelling in Earth's mantle convection system, and their interaction provides unique information on upwelling dynamics. I investigated the influence of the Iceland hotspot on the adjacent mid-Atlantic spreading center using phase-delay times of seismic surface waves, which show anomalous polarization anisotropy—a delay-time discrepancy between waves with different polarizations. This anisotropy implies that the hotspot induces buoyancy-driven upwelling in the mantle beneath the ridge.

The abundant volcanism at Iceland over the past 55 million years has been attributed to the presence of a high-temperature mantle plume (*1, 2*) that enhances the decompression melting associated with sea-floor spreading at the mid-Atlantic ridge (MAR). Although the impact of the plume on ridge dynamics is strongest on the Iceland plateau, a variety of observations imply that spreading and associated volcanism along the MAR south of Iceland (the Reykjanes Ridge or RR) have been modified by the hotspot. Specifically, the slow-spreading RR appears hotter than typical for the MAR: The sea floor formed at the RR is anomalously shallow (*3*), the topography of the RR is much smoother and lacks the segmentation and axial valley typical of slow-spreading centers (*4*), and the crust is anomalously thick (*5*). Moreover, the geochemistry of basalts erupted along the RR indicates mixing between an Icelandic plume source and the MAR source (*6, 7*). These observations imply that the plume affects ridge dynamics, perhaps via large-scale asthenospheric flow (*8–10*) and/or along-axis melt transport in the uppermost mantle and/or lower crust (*11*). The details of this plume-ridge interaction are poorly understood, however.

I investigated the dynamics of the RR system using seismic surface waves that traverse the ridge and adjacent oceanic lithosphere between the Gibbs Fracture Zone and Iceland (Fig. 1). Seventeen earthquakes with Richter magnitude between M_S 4.5 and M_S 6.6 (*12*) were recorded at the Global Seismic Network station BORG and up to 14 stations of the ICEMELT deployment (*1*). The surface waves from these events travel along and adjacent to the RR, and the travel times of these waves are sensitive to the average crust and upper-mantle velocity along each path. The paths are shorter than 1700 km, which means that the region is below the resolution limit of global models (*13–15*). To evaluate the travel times, I calculated synthetic seismograms for each event-station pair using a spherically symmetric isotropic seismic model appropriate for the near-ridge environment (*16*). The observed and synthetic seismograms were bandpass-filtered with corners at 10 and 45 mHz and had a dominant frequency of ~30 mHz.

School of Earth and Atmospheric Sciences, Georgia Institute of Technology, Atlanta, GA 30332, USA.

Inspection of these seismograms (Fig. 2) indicates that the vertically polarized Rayleigh waves arrive near the predicted time, but the transversely polarized Love waves are late. This discrepancy between the Love- and Rayleigh-wave propagation velocities indicates the presence of seismic anisotropy in the upper mantle. Such anisotropy is generally attributed to the alignment of olivine crystals by shear deformation associated with mantle flow (*17–19*). In particular, the *a* (fast) axes of olivine crystals tend to align in the flow direction, and the relative speeds of seismic waves with different propagation or polarization directions can be used to estimate flow orientation. In my data, the sign of the discrepancy (Love wave slower than Rayleigh wave) is opposite to that observed elsewhere (*14, 20–22*). To quantify these travel-time anomalies, I applied a cross-correlation procedure (*22–24*) to calculate frequency-dependent phase delays of both Love and Rayleigh waves relative to the synthetics. These phase delays characterize the dispersion of the surface waves at 5-mHz intervals (Fig. 2C), providing good sensitivity to seismic velocity structure to a depth of ~250 km (*22*). This process not only captured the magnitude of the Love-Rayleigh discrepancy, but also revealed a decrease in delay time (higher apparent velocity) with increasing lithospheric age.

Using more than 700 delay times, I constructed age-dependent anisotropic models of the uppermost mantle. The data were sorted by the average age of the propagation path [0 to 5 million years ago (Ma), 5 to 10 Ma, 10 to 15 Ma, 15 to 25 Ma, and 25 to 40 Ma], and phase delays in each age group were inverted for a one-dimensional, path-average model of radial anisotropy (*25*) using a linearized least-squares procedure (*22*). To facilitate comparison between structures of different ages, I varied only those parameters to which the data were most sensitive, the vertical and horizontal shear velocities (v_{SV} and v_{SH}); inversion tests indicated that compressional-velocity variations were not resolvable. The models consisted of seven layers between the base of the crust and 250 km depth, with linear changes in velocity within each layer and continuity required across layer boundaries. Crustal thickness along the path was fixed at 10 km (*5, 26*). I corrected the phase delays for errors in the event time and location using the *P*-wave delay times, and preferentially weighted the observations from southern Iceland by up to a factor of 2 to minimize the mapping of Icelandic structure onto the path models. The models explain more than 70% of the original data variance. Estimated errors in mean shear velocities are ±0.03 km/s, and shear anisotropy is resolved to within ~ $\pm1\%$. The 0- to 5-Ma model has larger errors (~ ±0.05 km/s and 1.5%) due to lower data quality along the ridge.

The models show a distinct pattern of shear anisotropy (Δv_S), with negative values ($v_{SV} > v_{SH}$) above ~100 km depth and positive values between ~100 to 200 km depth (Fig. 3). Negative anisotropy at shallow depths is required to satisfy the positive (late) phase delays for the horizontally polarized Love waves relative to the vertically polarized Rayleigh waves, whereas the deep, positive anisotropy is needed to fit the reversal of this trend at the lowest frequencies (Fig. 2C). The depth of this flip in sign is determined to within ±20 km. The anisotropy is small directly beneath the ridge (0 to 5 Ma), but by 5 to 10 Ma, it achieves values of –5% above 100 km and +4% below 100 km, and it remains unchanged at older ages to within the resolution of the data. This pattern of anisotropy is unlike that in comparable oceanic models, which display $\Delta v_S > 0$ throughout the upper 200 km of the mantle (*14, 20–22*) (Fig. 3).

If olivine fabric is the origin of the observed anisotropy, then the RR models imply that the olivine *a* axes are predominantly vertical above 100 km depth (*27*). Directly beneath the spreading center (0 to 5 Ma), this vertical fabric is probably associated with upwelling mantle flow. Such structure has been inferred in a global study (*28*) but has not been observed previously in detailed regional studies [e.g., (*20, 29, 30*)]. Off axis (age >5 Ma), the vertical fabric extends through the oceanic lithosphere, and I interpret it as ancient structure resulting from buoyancy-driven upwelling beneath the RR during lithosphere formation. Numerical models of sea-floor spreading imply two end-member scenarios for olivine fabric development. In systems where subaxial mantle flow is passively induced by plate spreading, the off-axis lithospheric fabric is largely horizontal and ridge-perpendicular as a result of the simple up-and-out pattern of flow (*18, 31*). Such models predict $\Delta v_S > 0$ and fast *P*- and Rayleigh-wave speeds in the spreading direction, both of which are consistent with previous observations [e.g., (*13, 17, 20–22, 28–30, 32*)]. The RR models are consistent with alternative models in which melt-zone upwelling is driven by buoyancy associated with retained melt, melt residuum, and/or locally hot mantle (*31*). Such models produce a tight circulation within the melting zone, and as the mantle material moves out of the spreading center, a near-vertical fabric associated with the downgoing limb of the circulation is retained in the off-axis lithosphere to a depth of ~60 km. Below this depth, the fabric becomes horizontal. The similarity between the numerical model of buoyancy-driven spreading and inferred anisotropy in the upper mantle beneath the north Atlantic is striking.

Buoyant upwelling is thought to be important beneath other slow-spreading ridges, in the form of discrete columns capable of producing along-axis crustal thickness variations associated with segmentation of bathymetry and gravity [e.g., (*33*)]. The RR lacks the characteristic features of segmented slow-spreading crust, however. Furthermore, in other slow-spreading regions of the Atlantic and Indian oceans where buoyant upwelling is inferred, seismic models show no hint of vertical lithospheric fabric (*14, 21, 32*). I hypothesize that the buoyant upwelling beneath the RR is anomalously strong; specifically, the source of the Iceland hotspot supplies heat to the RR, producing sufficient excess buoyancy to drive a sheet-like upflow beneath the ridge. The heat may be transferred via radial or ridge-parallel asthenospheric outflow from an Iceland plume (*8–10*); alternatively, it may be fed by a broad thermal anomaly in the upper mantle beneath the region (*15*). This scenario is consistent with the thickened crust, shallow bathymetry, minimal segmentation, and vertical lithospheric fabric. A temperature excess of ~50 K along the ridge is required to produce the observed crustal thickness and composition (*26*), and this value is consistent with my mean v_S models (Fig. 3). v_S increases with age as a result of plate cooling, but relative to the Pacific (*20*), this portion of the Atlantic is systematically slower at all ages. Part of this difference is probably anisotropic; horizontally propagating Love and Rayleigh waves travel ~1% slower in a structure with vertical olivine fabric than in one with horizontal fabric [e.g., (*34*)], and this slowness maps directly into the inferred mean v_S. Corrected for this difference, my models imply that the mean temperatures between 50 and 150 km depth beneath the RR are ~30 to 80 K higher than those beneath the Pacific spreading centers (*35*).

I considered alternative hypotheses to explain the anomalous anisotropy. One possibility is that spreading beneath the RR is so sluggish that the subaxial upwelling cools into the lithosphere before turning the corner. This scenario cannot explain the well-resolved increase in anisotropy between the 0- to 5-Ma and 5- to 10-Ma age groups, nor is it consistent with the high temperatures implied by the v_S profiles. Alternatively, a recent experiment (*36*) showed that the deformation of olivine under water-rich conditions may produce *a*-axis alignment nearly perpendicular to the flow plane. This implies that the anomalous anisotropy could be explained by passive spreading in a wet mantle. This hypothesis is also unlikely because the transition from $\Delta v_S < 0$ to $\Delta v_S > 0$ implies wet lithosphere overlying dry asthenosphere, which is opposite to what is expected [e.g., (*37*)]. Finally, perhaps the observed anisotropy results from partial melt trapped in vertical fractures or dikes within the oceanic lithosphere rather than olivine fabric (*29, 38*). The

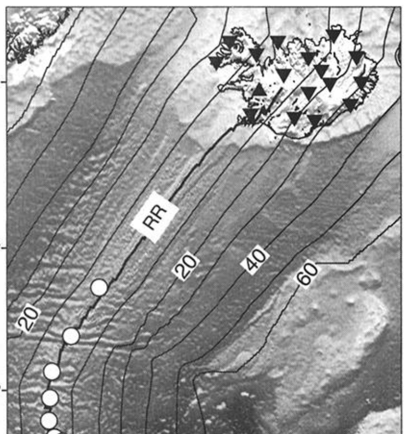

Fig. 1. Bathymetric map of the North Atlantic study region. Surface waves of earthquakes (open circles) from the Reykjanes Ridge (RR) and the Gibbs Fracture Zone (GFZ) were recorded on Iceland at BORG (triangle) and the ICEMELT stations (inverted triangles). Sea floor age is contoured at 20-Ma intervals.

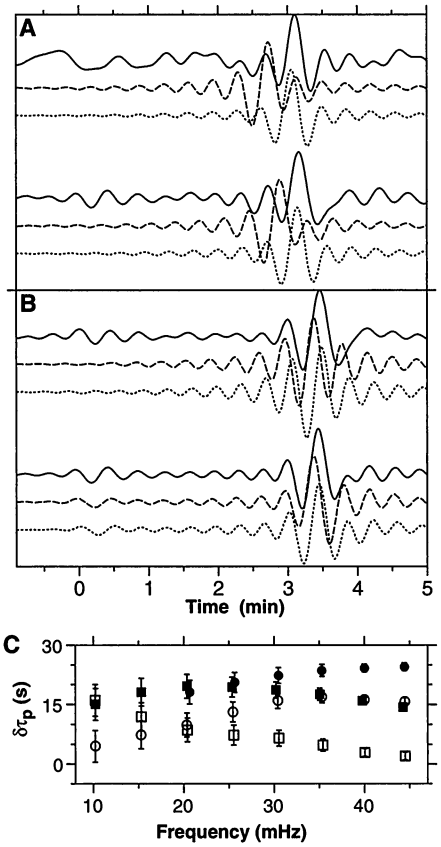

Fig. 2. Example seismograms and corresponding phase delays. In each set of three seismograms, the top trace (solid) is the observed data, the second trace (long dash) is the synthetic for an isotropic model, and the third trace (short dash) is the synthetic for the preferred anisotropic model. Within each panel, the top set corresponds to station BORG, the bottom set to ICEMELT station HOFF. Time scale is referenced to the predicted *P*-wave arrival time. **(A)** Tangential-component Love waves. **(B)** Vertical-component Rayleigh waves. **(C)** Phase delays as a function of frequency for the observed Love (circles) and Rayleigh (squares) waves, measured with respect to the isotropic model. Solid symbols are delay times for the BORG seismograms, which traverse lithosphere with a mean age of ~8 Ma; open symbols correspond to the HOFF seismograms, which traverse older lithosphere (~30 Ma).

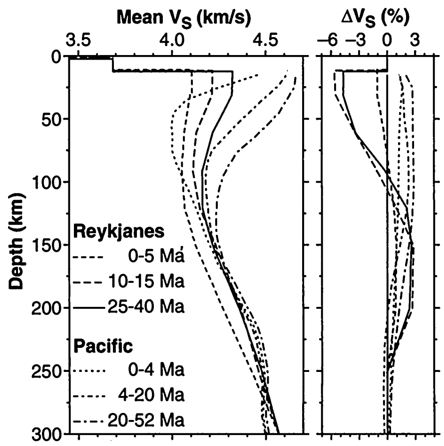

Fig. 3. Upper-mantle shear-velocity models of the Reykjanes region. Left panel, mean shear speed [$v_S = (v_{SH} + v_{SV})/2$]; right panel, shear anisotropy [$\Delta v_S = (v_{SH} - v_{SV})/v_S$]. Three age regions are shown for Reykjanes, as indicated; also shown are shear-velocity models for Pacific upper mantle (*20*) for three age regions.

observations that the anisotropy is weakest at the youngest ages (where melt content should be highest) and does not decay with age as the lithosphere cools are both inconsistent with this scenario. I conclude that the most likely explanation for the anomalous anisotropy is lithospheric fabric formed during hotspot-fueled buoyant upwelling at the RR.

This result has a number of implications for the dynamics of hotspot-ridge systems. It provides unique observational evidence that buoyancy-driven upwelling is an important component of ridge dynamics, especially in environments where passive sea-floor spreading is too slow to accommodate melt production. The presence of anomalous mantle fabric to a depth of ~100 km implies that the hotspot modulates upper-mantle dynamics beneath the ridge to at least this depth. Although I cannot directly estimate the temperature of the hotspot source, the 30- to 80-K anomaly inferred for the RR provides a constraint on temperature in numerical models of plume-ridge interaction. Finally, this result implies that the anisotropic structure of oceanic lithosphere may not be as simple as inferred through studies from the fast-spreading Pacific ridges, and that this structure holds important clues to ridge and plume dynamics.

References and Notes

1. C. J. Wolfe, I. T. Bjarnason, J. C. VanDecar, S. C. Solomon, *Nature* **385**, 245 (1997).
2. G. R. Foulger *et al.*, *Geophys. J. Int.* **142**, 1 (2000).
3. P. R. Vogt, *Earth Planet. Sci. Lett.* **13**, 153 (1971).
4. R. C. Searle *et al.*, *Earth Planet. Sci. Lett.* **160**, 463 (1998).
5. J. R. Smallwood, R. S. White, *J. Geophys. Res.* **203**, 5185 (1998).
6. J.-G. Schilling, *Nature* **242**, 565 (1973).
7. J. G. Fitton, A. D. Saunders, M. J. Norry, B. Hardarson, R. N. Taylor, *Earth Planet. Sci. Lett.* **153**, 197 (1997).
8. M. M. Yale, J. Phipps Morgan, *Earth Planet. Sci. Lett.* **161**, 45 (1998).
9. G. Ito, Y. Shen, G. Hirth, C. J. Wolfe, *Earth Planet. Sci. Lett.* **165**, 81 (1999).
10. G. Ito, *Nature* **411**, 681 (2001).
11. R. E. Bell, W. R. Buck, *Nature* **357**, 583 (1992).
12. Earthquake source parameters were obtained from Harvard University's Centroid Moment Tensor (CMT) catalog (www.seismology.harvard.edu).
13. J.-P. Montagner, T. Tanimoto, *J. Geophys. Res.* **96**, 20337 (1991).
14. G. Ekström, A. M. Dziewonski, *Nature* **394**, 168 (1998).
15. J. Ritsema, H. J. van Heijst, J. H. Woodhouse, *Science* **286**, 1925 (1999).
16. Synthetics were calculated via mode summation and were complete to 50 mHz, and perturbation theory was applied to correct each synthetic for the mean along-path bathymetry.
17. A. Nicolas, N. I. Christensen, in *Composition, Structure, and Dynamics of Lithosphere-Asthenosphere System*, K. Fuchs, C. Froidevaux, Eds., vol. 16 of *Geodynamics Series* (American Geophysical Union, Washington, DC, 1987), pp. 111–123.
18. N. M. Ribe, *J. Geophys. Res.* **97**, 8737 (1992).
19. S. Zhang, S.-I. Karato, *Nature* **375**, 774 (1995).
20. C. E. Nishimura, D. W. Forsyth, *Geophys. J.* **96**, 203 (1989).
21. J. J. Leveque, E. Debayle, V. Maupin, *Geophys. J. Int.* **133**, 529 (1998).
22. J. B. Gaherty, T. H. Jordan, L. S. Gee, *J. Geophys. Res.* **101**, 22291 (1996).
23. L. S. Gee, T. H. Jordan, *Geophys. J. Int.* **111**, 363 (1992).
24. This procedure calculates frequency-dependent phase delays and associated Frechet derivatives. It involves the cross-correlation of data and complete synthetics with a synthetic seismogram constructed for a target wave group, in this case fundamental mode surface waves. The method allows for consistent measurement and interpretation of phase delays, even in the case where substantial higher-mode energy is present.
25. Radial anisotropy is defined by five elastic parameters: the speeds of horizontally and vertically propagating *P* waves, $v_{PH}(z)$ and $v_{PV}(z)$; the speed of horizontally propagating, transversely polarized shear waves, $v_{SH}(z)$; the speed of a shear wave propagating horizontally with a vertical polarization or vertically with horizontal polarization, $v_{SV}(z)$; and a parameter that governs speeds at oblique propagation angles, $\eta(z)$. A complete description of the azimuthal anisotropy requires eight additional parameters [e.g., (*13*)], but we cannot resolve these terms because our data span a narrow azimuth range. Although there are tradeoffs between the radial and azimuthal terms that may bias the anisotropy estimate, the depth distribution is generally robust [e.g., (*34*)].
26. R. S. White, *Philos. Trans. R. Soc. London Ser. A* **355**, 319 (1997).
27. Olivine fabric with a predominantly horizontal orientation cannot preferentially enhance Rayleigh speeds because horizontally polarized Love waves are always relatively fast as well in such a medium (*34*).
28. H.-C. Nataf, I. Nakanishi, D. L. Anderson, *J. Geophys. Res.* **91**, 7261 (1986).
29. S. Webb, D. W. Forsyth, *Science* **280**, 1227 (1998).
30. C. J. Wolfe, S. C. Solomon, *Science* **280**, 1230 (1998).
31. D. K. Blackman *et al.*, *Geophys. J. Int.* **127**, 415 (1996).
32. G. Silveira, E. Stutzmann, D.-A. Griot, J.-P. Montagner, L. Mendes Victor, *Phys. Earth Planet. Inter.* **106**, 257 (1998).
33. K. Barnouin-Jha, E. M. Parmentier, D. W. Sparks, *J. Geophys. Res.* **102**, 11979 (1997).
34. V. Maupin, *Geophys. J. R. Astron. Soc.* **83**, 379 (1985).
35. I calculated this temperature anomaly by comparing my 10- to 15-Ma model with a 4- to 20-Ma Pacific model (*20*). Between 50 and 150 km depth, the Reykjanes model is 70 m/s slower than the Pacific. Correcting this for the slowing effects of vertical fabric in the Reykjanes region reduces the velocity difference to 15 to 40 m/s. The temperature range is calculated assuming $\delta v_S/\delta T = -0.5$ m s^{-1} K^{-1}.
36. H. Jung, S.-I. Karato, *Eos (Fall Suppl.)* **81**, F1209 (2000).
37. G. Hirth, D. L. Kohlstedt, *Earth Planet. Sci. Lett.* **144**, 93 (1996).
38. J. W. Schlue, L. Knopoff, *Geophys. J. R. Astron. Soc.* **49**, 145 (1977).
39. Tabular and graphical representations of all five RR models are provided as supplemental data on *Science* Online (www.sciencemag.org/cgi/content/full/293/5535/1645/DC1).

40. Data were provided by Y. Shen and the IRIS Data Management Center (www.iris.washington.edu). I thank G. Hirth and D. Lizarralde for useful discussions. Supported by NSF grant EAR-9814565.

12 April 2001; accepted 18 July 2001

Climate Change as the Dominant Control on Glacial-Interglacial Variations in C_3 and C_4 Plant Abundance

Y. Huang,[1*] F. A. Street-Perrott,[2] S. E. Metcalfe,[3] M. Brenner,[4] M. Moreland,[5] K. H. Freeman[5]

Although C_4 plant expansions have been recognized in the late Miocene, identification of the underlying causes is complicated by the uncertainties associated with estimates of ancient precipitation, temperature, and partial pressure of atmospheric carbon dioxide (P_{CO_2}). Here we report the carbon isotopic compositions of leaf wax *n*-alkanes in lake sediment cores from two sites in Mesoamerica that have experienced contrasting moisture variations since the last glacial maximum. Opposite isotopic trends obtained from these two sites indicate that regional climate exerts a strong control on the relative abundance of C_3 and C_4 plants and that in the absence of favorable moisture and temperature conditions, low P_{CO_2} alone is insufficient to drive an expansion of C_4 plants.

Plants use two principal carbon fixation pathways, the C_3 and C_4 cycles, during photosynthesis (*1*). C_4 plants (notably tropical grasses) are disadvantaged relative to C_3 plants (such as trees, shrubs, and cool-climate grasses) at high CO_2/O_2 ratios because of the additional energy expense needed to concentrate CO_2 in the bundle-sheath cells. At low CO_2/O_2, however, C_4 plants can achieve a relatively high quantum yield by suppressing photorespiration. The evolution of C_4 photosynthesis reflects an adaptation to the declining CO_2/O_2 ratio in Earth history (*2*). Based on this principle, expansions of C_4 plants in the late Miocene (*3*), Cretaceous (*4*), and last glacial maximum (LGM) (*5*, *6*) have been attributed

[1]Department of Geological Sciences, Brown University, Providence, RI 02912, USA. [2]Department of Geography, University of Wales Swansea, Swansea, SA2 8PP, UK. [3]Department of Geography, University of Edinburgh, Edinburgh, EH8 9XP, UK. [4]Department of Geological Sciences, University of Florida, Gainesville, FL 32611, USA. [5]Department of Geosciences, Pennsylvania State University, State College, PA 16802, USA.

*To whom correspondence should be addressed.